Resistance to PI3Kδ inhibitors in marginal zone lymphoma can be reverted by targeting the IL-6/PDGFRA axis

Alberto J. Arribas,[1,2*] Sara Napoli,[1*] Luciano Cascione,[1,2] Giulio Sartori,[1] Laura Barnabei,[1] Eugenio Gaudio,[1] Chiara Tarantelli,[1] Afua Adjeiwaa Mensah,[1] Filippo Spriano,[1] Antonella Zucchetto,[3] Francesca M. Rossi,[3] Andrea Rinaldi,[1] Manuel Castro de Moura,[4] Sandra Jovic,[5] Roberta Bordone-Pittau,[6] Alessandra Di Veroli,[7] Anastasios Stathis,[6,8] Gabriele Cruciani,[7] Georg Stussi,[6] Valter Gattei,[3] Jennifer R. Brown,[9] Manel Esteller,[4,10-12] Emanuele Zucca,[1,6] Davide Rossi[1,6] and Francesco Bertoni[1,6]

[1]Institute of Oncology Research, Faculty of Biomedical Sciences, Università della Svizzera Italiana, Bellinzona, Switzerland; [2]SIB Swiss Institute of Bioinformatics, Lausanne, Switzerland; [3]Centro di Riferimento Oncologico di Aviano – CRO, Aviano, Italy; [4]Josep Carreras Leukemia Research Institute (IJC), Badalona, Spain; [5]Institute for Research in Biomedicine, Università della Svizzera italiana, Bellinzona, Switzerland; [6]Oncology Institute of Southern Switzerland, Bellinzona, Switzerland; [7]Department of Chemistry, Biology and Biotechnology, University of Perugia, Perugia, Italy; [8]Faculty of Biomedical Sciences, Università della Svizzera Italiana, Bellinzona, Switzerland; [9]Chronic Lymphocytic Leukemia Center, Division of Medical Oncology, Dana-Farber Cancer Institute and Harvard Medical School, Boston, MA, USA; [10]Centro de Investigacion Biomedica en Red Cancer (CIBERONC), Madrid, Spain; [11]Institucio Catalana de Recerca i Estudis Avançats (ICREA), Barcelona, Spain and [12]Physiological Sciences Department, School of Medicine and Health Sciences, University of Barcelona (UB), Barcelona, Spain.

**AJA and SN contributed equally as co-first authors.*

Correspondence: A. Arribas
alberto.arribas@ior.usi.ch

F. Bertoni
francesco.bertoni@ior.usi.ch

Received: September 4, 2021.
Accepted: April 12, 2022.
Prepublished: April 28, 2022.

https://doi.org/10.3324/haematol.2021.279957

Resistance to PI3Kδ inhibitors in marginal zone lymphoma can be reverted by targeting the IL-6/PDGFRA axis

Alberto J. Arribas [1,2*#], Sara Napoli [1*], Luciano Cascione [1,2], Giulio Sartori [1], Laura Barnabei [1], Eugenio Gaudio [1], Chiara Tarantelli [1], Afua Adjeiwaa Mensah [1], Filippo Spriano [1], Antonella Zucchetto [3], Francesca M Rossi [3], Andrea Rinaldi [1], Manuel Castro de Moura [4], Sandra Jovic [5], Roberta Bordone Pittau [6], Alessandra Di Veroli [7], Anastasios Stathis [6,8], Gabriele Cruciani [7], Georg Stussi [6], Valter Gattei [3], Jennifer R Brown [9] , Manel Esteller [4,10-12], Emanuele Zucca [1,6], Davide Rossi [1,6], Francesco Bertoni [1,6#].

[1] Institute of Oncology Research, Faculty of Biomedical Sciences, USI, Bellinzona, Switzerland; [2] SIB Swiss Institute of Bioinformatics, Lausanne, Switzerland; [3] Centro di Riferimento Oncologico di Aviano – CRO, Aviano, Italy; [4] Josep Carreras Leukaemia Research Institute (IJC), Badalona, Barcelona, Catalonia, Spain; [5] Institute for Research in Biomedicine, Università della Svizzera italiana, Bellinzona, Switzerland; [6] Oncology Institute of Southern Switzerland, Bellinzona, Switzerland; [7] Department of Chemistry, Biology and Biotechnology, University of Perugia, Perugia, Italy; [8] Faculty of Biomedical Sciences, USI, Bellinzona, Switzerland; [9] Chronic Lymphocytic Leukemia Center, Division of Medical Oncology, Dana-Farber Cancer Institute and Harvard Medical School, Boston, MA, USA; [10] Centro de Investigacion Biomedica en Red Cancer (CIBERONC), Madrid, Spain: [11] Institucio Catalana de Recerca i Estudis Avançats (ICREA), Barcelona, Catalonia, Spain: [12] Physiological Sciences Department, School of Medicine and Health Sciences, University of Barcelona (UB), Barcelona, Catalonia, Spain.

*, equally contributed

#, co-corresponding authors

Supplementary materials and methods

Treatments

Response to single or drug combination treatments was assessed upon 72hr of exposure to increasing doses of drug followed by MTT assay. Cells were plated in 96-well plates at a concentration of 10,000 per well in non-phenol RPMI-1640 (Gibco Invitrogen, Basel, Switzerland) supplemented with 10% fetal bovine serum (Gibco) and 1% penicillin-streptomycin (Gibco). After 4 hours of seeding, cells were exposed treatments. Sensitivity to single drug treatments was evaluated by IC50 (4-parameters calculation upon log-scaled doses) and area under the curve (PharmacoGX R package (1)) calculations. The beneficial effect of the combinations versus the single agents was considered both as synergism according to the Chou-Talalay combination index, as previously described (2), and as potency and efficacy according to the MuSyC algorithm (3). For conditioned medium experiments, parental cells were cultured with 48h-conditioned medium from idelalisib-resistant, washed out in PBS and underwent MTT proliferation assay. Z-test was performed to determine statistically significant differences in drug response experiments ($p<0.05$).

Flow Cytometry (FACS) and protein analyses

Surface expression of PDGFRA, IL-6R, IL-6ST, CXCR4 and CD19 (Table S1) were measured as previously described (4). Levels of p-AKT, p-BTK, p-PLCG2, p-mTOR and p-ERK were determined as previously described (5) (Table S2). Cell cycle was analyzed by FACS (cells fixed 72 hrs after treatments, propidium iodide staining), percentages of cell cycle phases (sugG0, G0-G1, S, G2/M) were obtained analyzing DNA histograms with the flowCore R package (6).

Immunoblotting was performed to determine the expression of AKT/p-AKT, ERK/p-ERK JAK/p-JAK, STAT/p-STAT and GAPDH (Table S3). Protein extraction, separation, and immunoblotting were performed as previously described (2).

Genomics

For whole exome sequencing (WES), genomic DNA was enriched in protein coding sequences using the exome capture SureSelect XT library preparation (v6, 58 Mb; Agilent Technologies), according to the manufacturer's protocol. The captured targets were subjected to next generation sequencing using the HiSeq 2500 analyzer (Illumina) with the paired-end 2x125 bp read option, following the manufacturer's instructions, to obtain a 14x coverage. Exome capture and next generation sequencing were performed at the HiSeq Service of Fasteris SA (Plan-les-Ouates, Switzerland).

Transcriptome sequencing (RNA-Seq) was done using the TruSeq RNA Sample Prep Kit v2 for Illumina (Illumina, San Diego, CA, USA) as previously described (7).

For small RNA-Seq, cDNA libraries were assembled using total RNA prepared using the SMARTer smRNA-Seq Kit for Illumina (Clontech Laboratories, Inc. USA). Briefly, the total RNA suspension was polyadenylated by the Poly(A) Polymerase at 16°C for 5 minutes on a thermal cycler, then cDNA synthesized using PrimeScript Reverse Transcription, primed by the 3' smRNA dT primer. cDNA was amplified and full-length Illumina adapters were added via PCR. PCR products were purified using the NucleoSpin Gel and PCR Clean-Up kit. Libraries were amplified using 10 cycles of PCR on thermocycler, then quantified on a Qubit 4 Fluorometer (Invitrogen, USA) and analyzed on an Agilent Bioanalyzer High Sensitivity DNA chip for qualitative control. The cDNA libraries were size selected to enrich for <150bp using Agencourt AMPure XP beads, first selection with a (0.8X) of beads and second selection with a (2.2X) of beads. Libraries were then sequenced on a NextSeq500 Illumina using 75 cycles.

Methylation profiling was done using the MethylationEPIC BeadChip Infinium following the manufacturer's instructions for the automated processing of arrays with a liquid handler (Illumina Infinium HD Methylation Assay Experienced User Card, Automated Protocol 15019521 v01), as previously described (8).

Data mining

For WES, quality control on raw reads was performed with FastQC (9). Paired-end reads were aligned to human reference sequence GRCh37 using the Burrows–Wheeler Aligner (BWA version 0.6.1) (10). Potential PCR duplicates were removed using SAM tools command (11). Mapping quality score recalibration and local realignment around insertions and deletions (indels) were performed using the Genome Analysis Toolkit (GATK) (12). Single nucleotide variants and small indels were called separately using the GATK Unified-Genotyper (13). Annovar tool (14) was used for functional annotation of variants, and all mutations found were manually checked and explored using the Integrative Genomic Viewer 2.03 (15). The list of putative acquired variants was identified using the following filtering constrains. Mutations present in the parental cell lines were excluded, as well as known germline variants reported at dbSNP137 and the 1000 Genomes Project (16). We considered of our interest exonic and nonsynonymous variants, including stop-gain single nucleotide variants, splicing, and frameshift indels. We excluded non-exonic variants and synonymous mutations. We also retained variants already reported in the COSMIC database (17). Since samples underwent both whole exome sequencing and RNA-sequencing, variants were also investigated for the correspondence between whole exome and RNA-sequencing. Finally, only variants transcribed to RNA were considered for further analyses.

For RNA-Seq, data were analyzed as previously described (7). Differentially expressed genes were calculated with moderated t-test on RNA-seq. The false discovery rate (FDR, Benjamin-Hochberg correction) was calculated to control for false positives. FDR <0.05 and absolute fold-change higher than 2 was considered significant. Functional analysis was performed on the collapsed gene symbol list using GSEA (Gene Set Enrichment Analysis) with the MSigDB (Molecular Signatures Database) C2-C7 gene sets (18, 19), and SignatureDB database (https://lymphochip.nih.gov/signaturedb/).

Statistical tests were performed using the R environment (R Studio console; RStudio, Boston, MA, USA).
For small RNA-Seq, we first carried out a pre-processing step with Cutadapt (20) to identify and remove all of non-biological part of the reads (adapters). Then, a quality control step was performed using FastQC where we collected key information about the quality of sequencing reads including quality score distribution along the reads, GC content, read length, and level of sequence duplication. Once the FASTQ files have been validated, BWA aligned the reads to the human reference genome (hg38). We then quantified the known microRNAs present in miRBase (21), counting the reads mapped to their loci with featureCounts (22). We set the -O flag to have reads that map to several overlapping microRNAs assigned to all of them. We also set the -s parameter to 1 to only count reads that map to the same strand as the microRNA, and the -M flag to make sure we count multi mapping reads. We compensated for different sequencing depths using the TMM normalization (normalization step), and calculated the log2 counts-per million values (lcpm). Log count-per-million values were inputed to principal component analysis (PCA) or multi-dimensional scaling plot to get a global look of how similar the microRNA expression profiles are in the different samples. Limma identified the modulated miRNAs between the two phenotypes of interest.
For methylation profiling, the DNA methylation beta values were obtained from the raw IDAT files by using the minfi package in R. The data was normalized with the ssNoob method and positions with a detection P-value greater than 0.01, NoCG Start as well as probes with SNPs, multihit start probes and XY chromosome probes were removed from the analysis. The differentially methylated positions between groups with a Benjamini-Hochberg adjusted p-value lower than 0.05 and an absolute methylation difference greater than 0.3 were selected from a linear model calculated with the limma R package.
Finally, unsupervised multidimensional scaling plot were used to visualize resistant and parental multi-omics profiles.

Gene silencing

Small interfering RNAs were used for gene expression silencing. The control siRNA pool, human IL-6 siRNA pool and human PDGFRA siRNA pool 200 pmol were purchased (Dharmacon GE Healthcare, Horizon Discovery Ltd., Cambridge, UK). VL51 cells (1 million per sample) were transfected with siRNA pools (200 pmol), or 100 pmols of each pool when silencing both IL-6 and PDGFRA, using 4D Nucleofector (Amaxa-Lonza, Basel, Switzerland), with protocol CM-150, according to manufacturer instructions, and incubated for 48h to check RNA downregulation and 72h to check effect on proliferation.

Supplementary tables

Table S1

Protein	fluorochrome	company	# catalog
PDGFRA	FITC	Santa Cruz	398206
	2nd ab	Dako	F0479
CD126 (IL6R)	PE	BD Bioscience	561696
CD130 (IL6ST)	PerCP-Cy5.5	BD Bioscience	746079
CD184 (CXCR4)	PE	BD Bioscience	561733
CD19	PE-Cy7	Beckman Coulter	IM3628

Table S1. Panel of surface markers tested in the immunophenotyping experiments of parental and resistant cells by flow cytometry.

Table S2

protein	fluorochrome	company	# catalog
ERK 1/2 (pT202/Y204)	Alexa488	BD Biosciences	612592
BTK (pY223)	PE	BD Biosciences	562753
PLCγ (pY759)	PE	BD Biosciences	558490
AKT (pS473)	Alexa647	BD Biosciences	560343
mTOR (pS2448)	Alexa647	BD Biosciences	564242

Table S2. Panel of kinases analyzed in the Phospho Flow experiments of parental and resistant cells by flow cytometry.

Table S3

source	protein	company	# catalog
rabbit polyclonal	α-AKT	Cell Signaling	9272
rabbit polyclonal	α-p(S473) AKT	Cell Signaling	4060
rabbit polyclonal	α-ERK1/2	Cell Signaling	4696
rabbit polyclonal	α-p(Y204) ERK	Santa Cruz	7383
rabbit monoclonal	α-JAK2	Cell Signaling	3230
rabbit polyclonal	α-p(Y1007/1008) JAK2	Cell Signaling	3771
rabbit monoclonal	α-STAT3	Cell Signaling	9139
rabbit monoclonal	α-p(Y705) STAT3	Cell Signaling	9131
rabbit monoclonal	α-p(S727) STAT3	Cell Signaling	9136
mouse monoclonal	α-GAPDH	CNIO	FF26A/F9

Table S3. Panel of proteins tested in the immunoblotting experiments of parental and resistant cells by western blotting.

Table S4 (Excel file). Whole exome sequencing data, including single nucleotide variants and copy number variants.

Table S5 (Excel file). Multi-omics analyses. Output tables of the moderated t-tests comparing transcriptome, microRNA and methylation profiles of resistant and parental for VL51 models. Output results of Gene Set Enrichment Analysis comparing GEP data of resistant and parental for VL51 models

Table S6 (Excel file). Clinical information on the series of serum samples from CLL clinical patients exposed to idelalisib. Samples were longitudinally acquired at different time points. Patients were paired according to similar clinical features.

Supplementary Figures

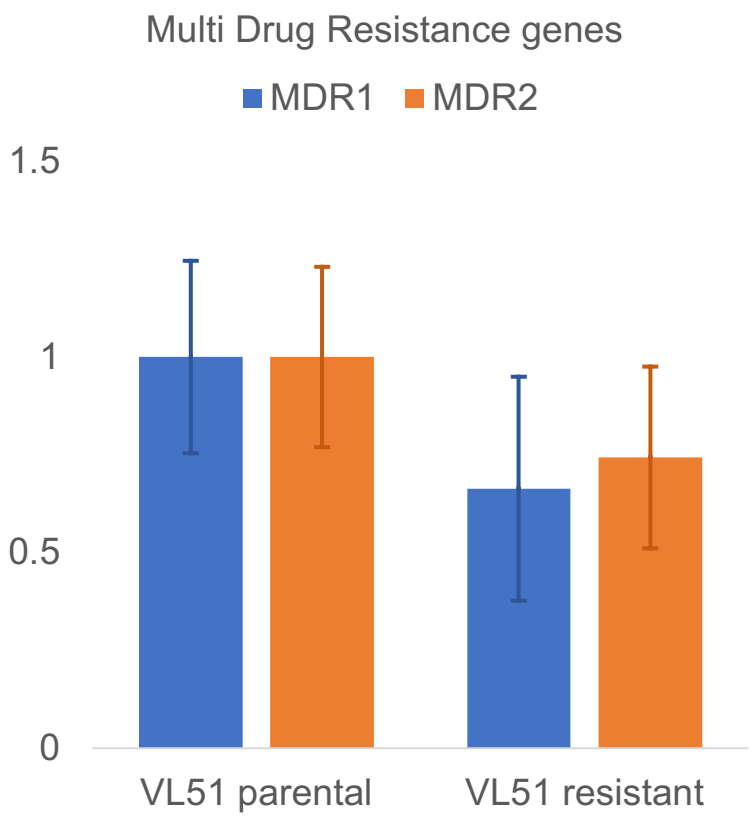

Figure S1. Multi drug resistance phenotype was ruled out by the expression of MDR1 (blue) and MDR2 (orange) genes by real time PCR. Data derived from two independent experiments; error bars represent standard deviation of the mean.

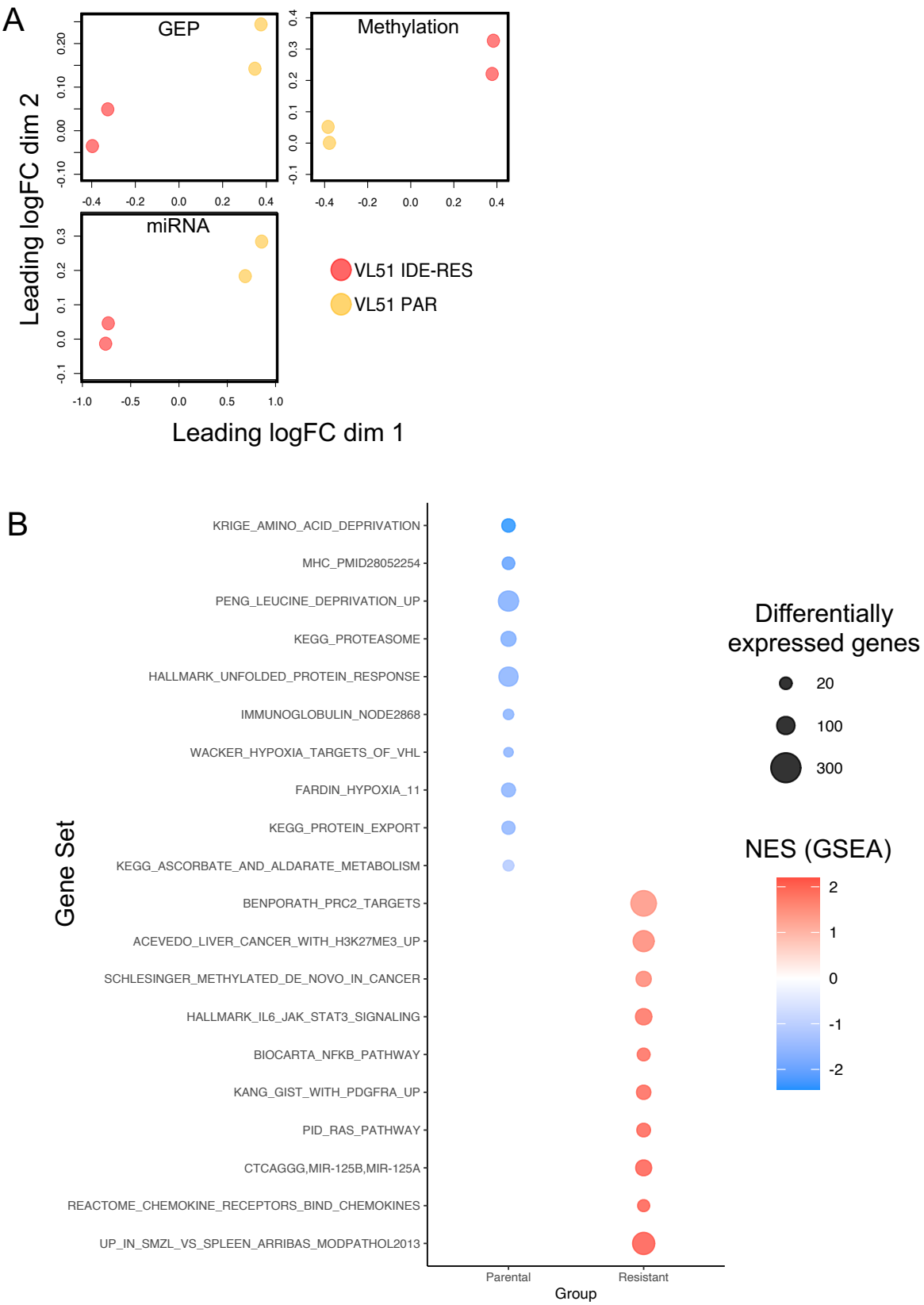

Figure S2. (A) Multidimensional scaling plot showing a 2-dimensional projection of distances across parental and resistant clones for RNA (GEP, top left), methylation (top right) and miRNA (bottom left) profiles. Red dots for resistant and yellow for parental. (B) Gene set enrichment analyses (GSEA, Broad Institute) comparing parental and resistant per each line. Statistically significant differences with values of absolute NES higher than1, P <0.05 and FDR <0.25.

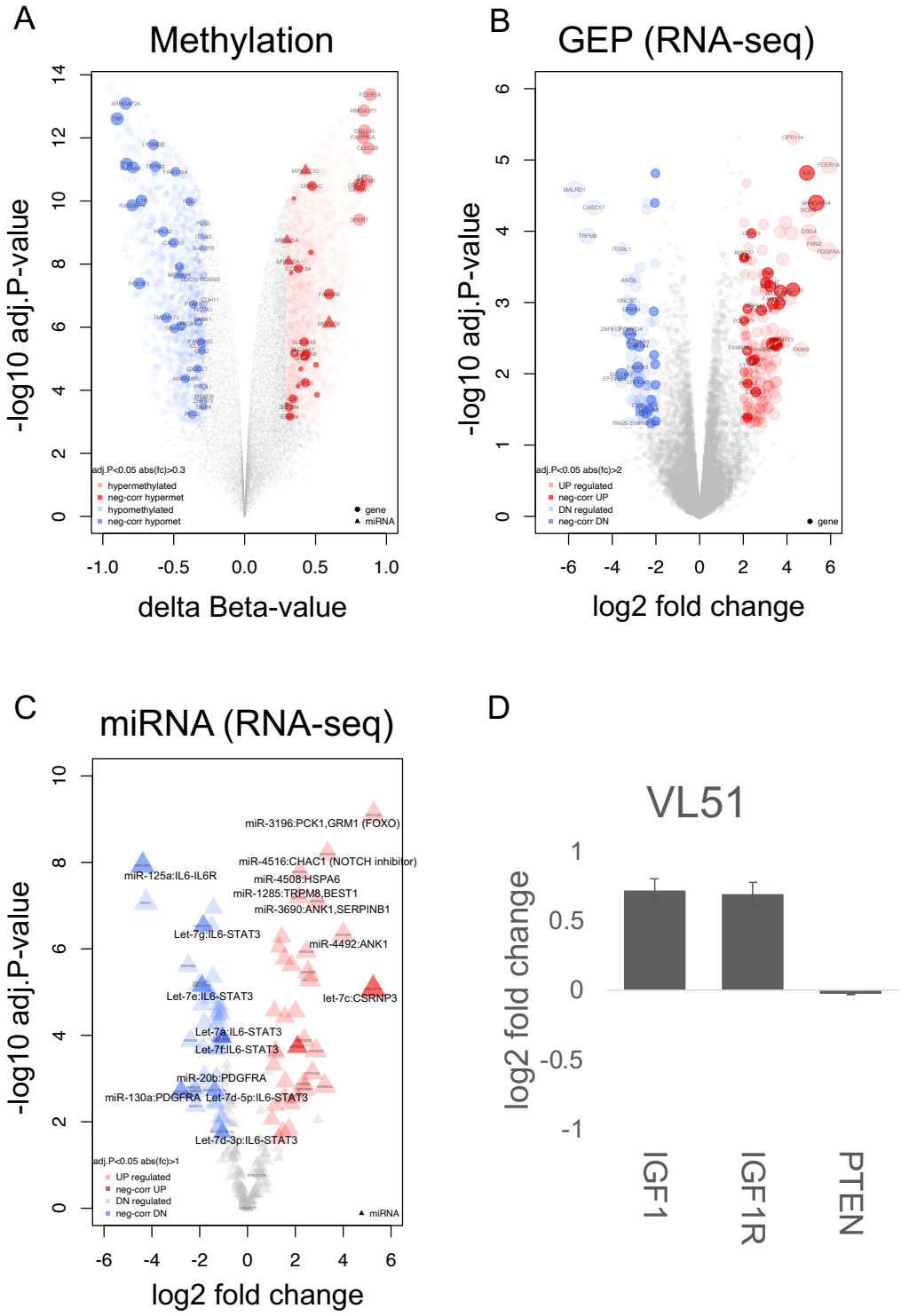

Figure S3. Vulcano plots on methylation (A), gene expression (RNA-seq, B) and microRNA (RNA-seq, C) profiles of VL51 resistant compared to parental. Moderated t-test (limma R Package) was performed comparing VL51 resistant to parental: delta Beta-value (methylation), fold change (RNA-seq), adj.P-value for Bonferroni correction of the nominal p-value. Dots represents genes and triangles represent miRNAs. Red corresponds to higher values in resistant, and blue higher values in parental. The genes or miRNAs inversely correlated with methylation are highlighted in darker color: hypomethylated and overexpressed in dark red (neg-corr UP) and hypermethylated and repressed in dark blue (neg-corr-DN). (D) RNA expression of IGF1, IGF1R and PTEN in parental and resistant of VL51 lines. Bars represents log2-scaled fold change by RNA-seq, * for statistically significant differences.

A

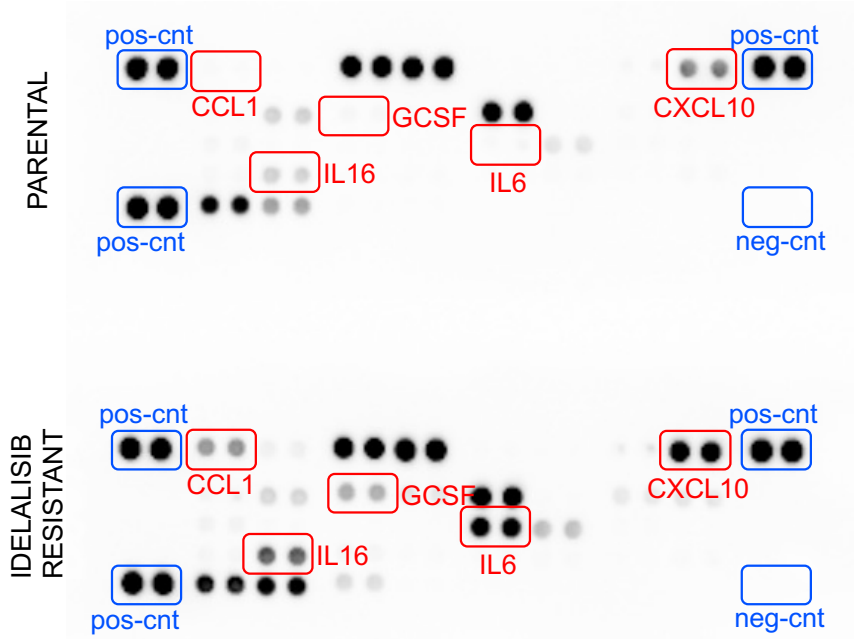

Cytokine array upon 72hrs conditioned media (ELISA)

B

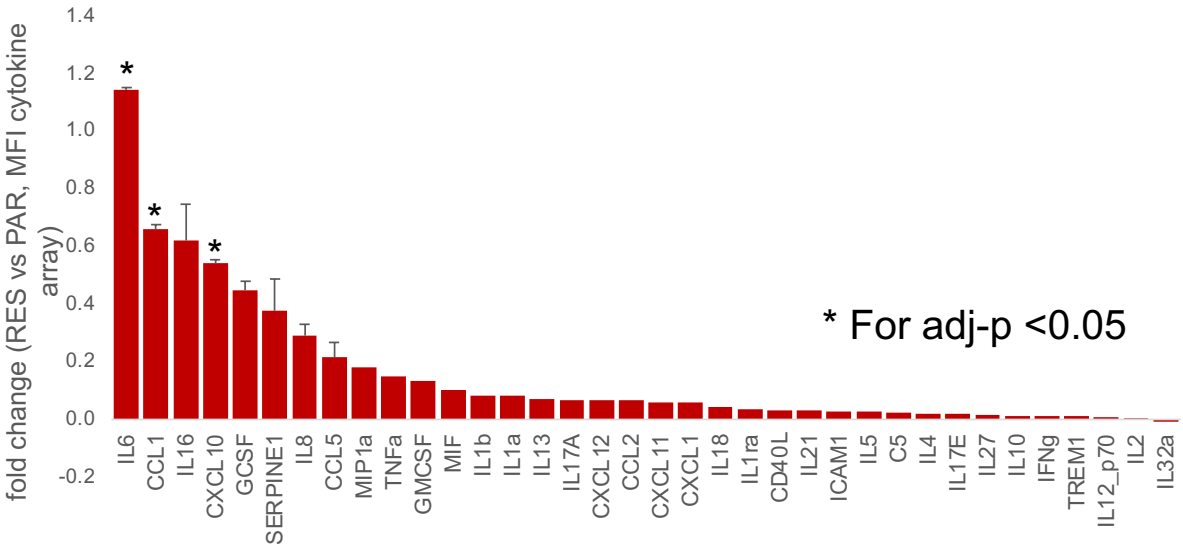

Figure S4. Secreted levels of cytokines were measured using the Proteome Profiler Human Cytokine Array Kit (R&D Systems) following the manufacturer's protocol. (A) Membrane for parental (top panel) and idelalisib resistant (bottom panel) conditioned media. (B) Fold change between resistant and parental for the quantification of the cytokine array membranes. Error bars represents standard deviation of the mean.

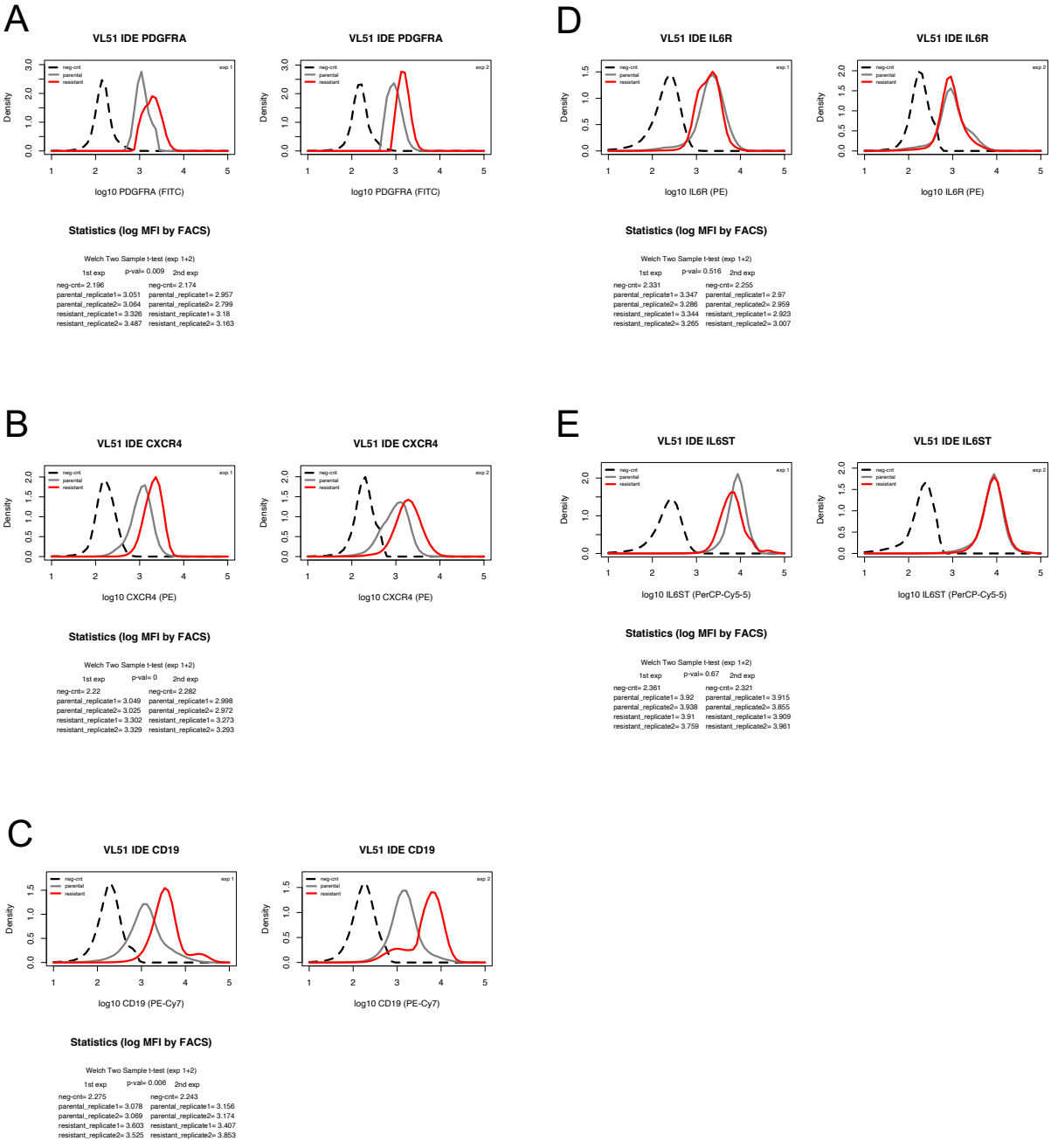

Figure S5. Expression levels of surface PDGFRA (A), CXCR4 (B), CD19 (C), CD126 (IL6R, D) and CD130 (IL6ST, E) was measured by FACS in VL51 parental and resistant. Two independent experiments were performed: exp1 (left panel) and exp2 (right panel). Density plots show the median MFI values of two replicates from each experiment: negative control (dotted black), parental (grey), resistant (red). Results are presented from Welch Two Sample test performed on MFI values of the two experiments.

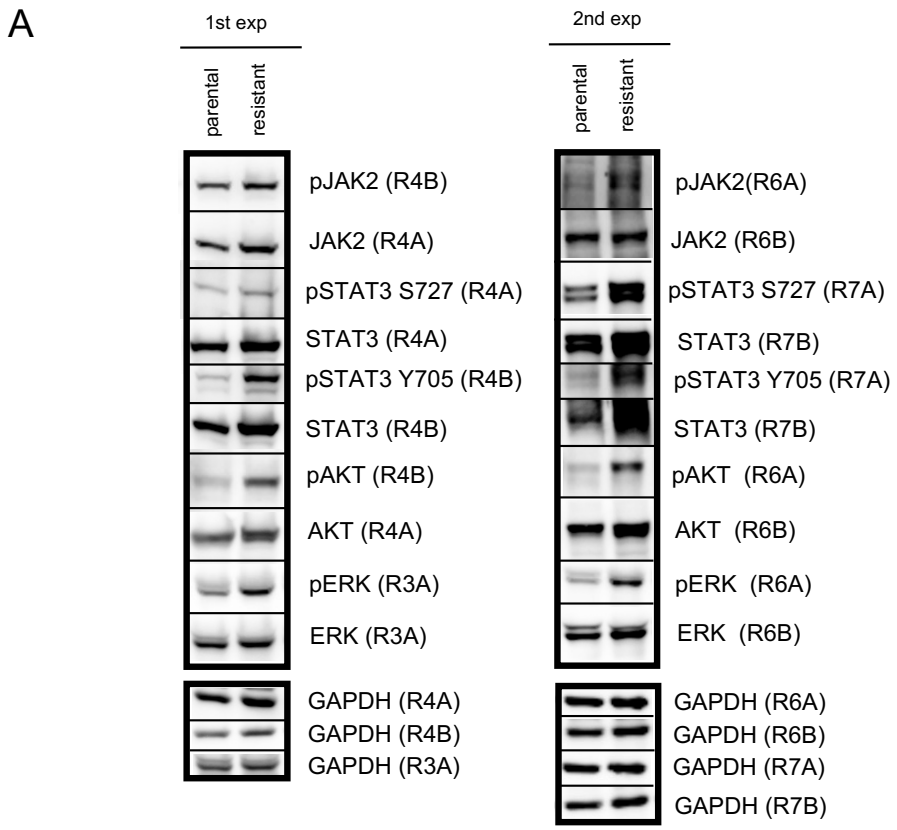

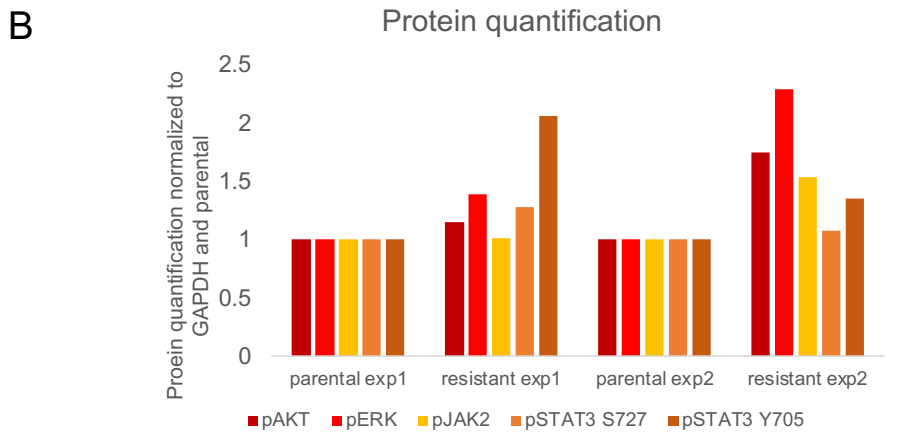

protein	mean	standard error of the mean	experiment 1	experiment 2	experiment 1	experiment 1	experiment 2	experiment 2	statistics
			fold change compared to parental	fold change compared to parental	protein quantification parental (normalized to GAPDH and parental)	protein quantification resistant (normalized to GAPDH and parental)	protein quantification parental (normalized to GAPDH and parental)	protein quantification resistant (normalized to GAPDH and parental)	t-test p-value: parental vs resistant
pAKT	0.448	0.150	0.147	0.749	1	1.147	1	1.749	0.052
pERK	0.841	0.226	0.389	1.294	1	1.389	1	2.294	0.034
pJAK2	0.276	0.130	0.016	0.536	1	1.016	1	1.536	0.096
pSTAT3 S727	0.179	0.051	0.281	0.078	1	1.281	1	1.078	0.040
pSTAT3 Y705	0.706	0.178	1.061	0.351	1	2.061	1	1.351	0.030

Statistically significant differences highlighted in yellow

Figure S6. (A) Immunoblotting was performed to measure protein levels in parental and resistant clones for pJAK2/JAK2, pSTAT3/STAT3 S727, pSTAT3/STAT3 Y705, pAKT/AKT and pERK/ERK (A). GAPDH was used as a loading control. (B) Protein quantification was done normalizing first to GAPDH and then to parental. Figure shows two independent experiments. Mean and standard error correspond to fold change of resistant compared to parental in the two experiments.

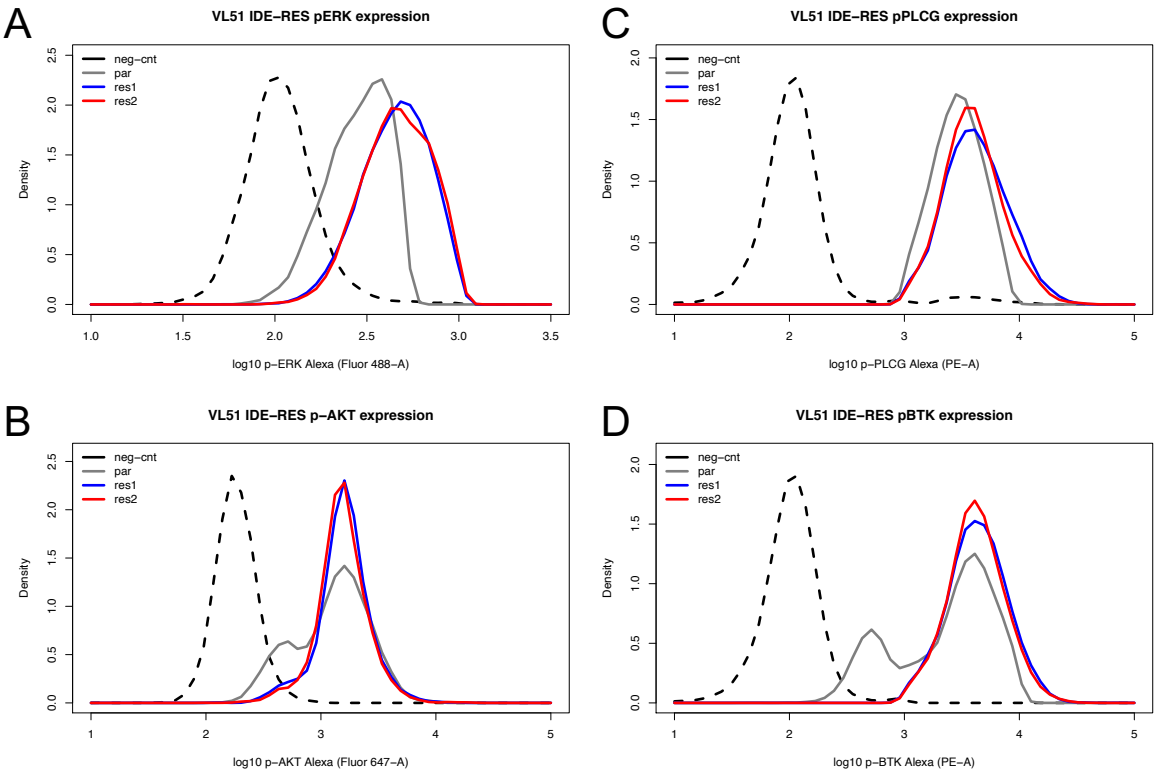

Figure S7. Levels of p-ERK (A), p-AKT (B), p-PLCG (C) and p-BTK (D) were determined as previously described (5) in VL51 parental and resistant. Density plots show the median MFI values of two independent experiments: negative control (dotted black), parental (grey), resistant (blue and red).

A

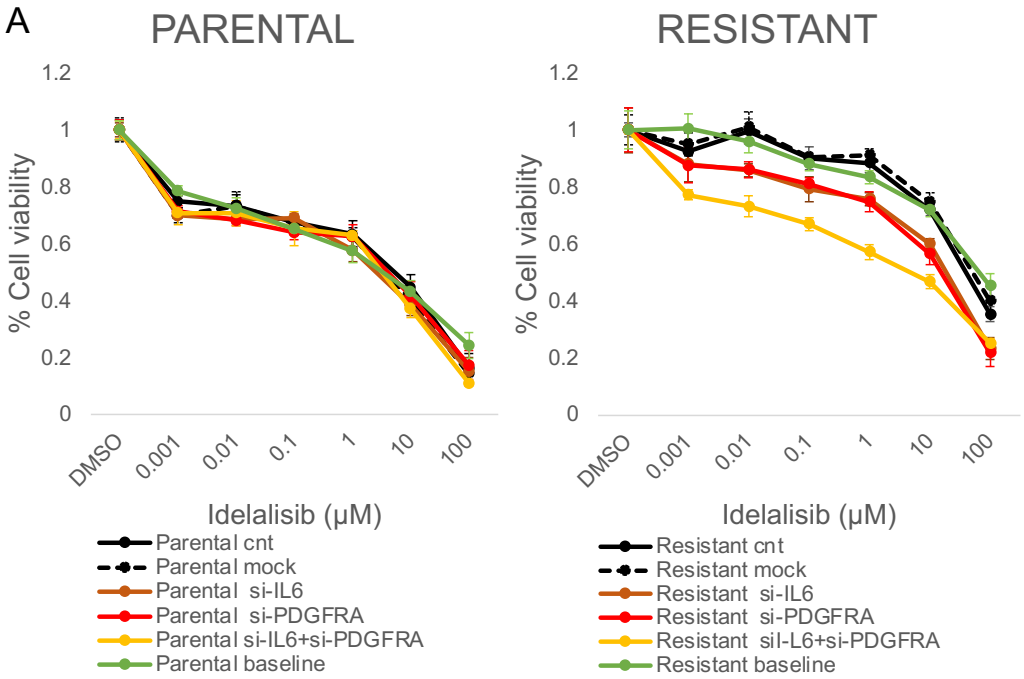

B

			siRNA experiment							siRNA experiment			
	Idelalisib (μM)	Parental baseline	Parental cnt	Parental mock	Parental si-IL6	Parental si-PDGFRA	Parental si-IL6+si-PDGFRA	Resistant baseline	Resistant cnt	Resistant mock	Resistant si-IL6	Resistant si-PDGFRA	Resistant siI-L6+si-PDGFRA
mean of three independent experiments	0	1.00	1.00	1.00	1.00	1.00	1.00	1.00	1.00	1.00	1.00	1.00	1.00
	0.001	0.79	0.75	0.70	0.70	0.71	0.71	1.00	0.92	0.95	0.88	0.88	0.77
	0.01	0.72	0.73	0.73	0.69	0.68	0.71	0.96	1.00	1.01	0.86	0.86	0.73
	0.1	0.65	0.68	0.67	0.69	0.64	0.65	0.88	0.90	0.91	0.79	0.81	0.67
	1	0.58	0.63	0.62	0.58	0.63	0.63	0.83	0.88	0.91	0.76	0.75	0.57
	10	0.43	0.45	0.40	0.39	0.42	0.37	0.72	0.72	0.75	0.60	0.56	0.47
	100	0.24	0.16	0.14	0.15	0.17	0.11	0.45	0.35	0.40	0.23	0.22	0.25
statistics (p-value from Z-test)	vs Parental baseline		0.545	0.488	0.452	0.477	0.450	0.012	0.017	0.012	0.118	0.127	0.527
	vs Parental cnt	0.545		0.494	0.459	0.484	0.458	0.031	0.041	0.030	0.120	0.137	0.425
	vs Parental mock	0.488	0.494		0.515	0.541	0.512	0.011	0.015	0.011	0.222	0.240	0.465
	vs Resistant baseline	0.012	0.013	0.011	0.009	0.010	0.010		0.474	0.473	0.102	0.097	0.013
	vs Resistant cnt	0.017	0.018	0.015	0.013	0.013	0.014	0.474		0.441	0.105	0.113	0.017
	vs Resistant mock	0.012	0.013	0.011	0.009	0.009	0.010	0.473	0.441		0.095	0.091	0.012

Statistically significant differences highlighted in yellow

Figure S8. Small interfering RNAs were used for gene expression silencing of IL6 (brown), PDGFRA (red), and IL6+PDGFRA (orange). Then sensitivity to idelalisib was tested by MTT assay upon 72hr. (A) Drug-response curves of parental (left) and resistant (right), and (B) heatmap of cell viability values correspond of the mean of three independent experiments. Parental and resistant baseline (green lines in (A), and highlighted in grey in (B) correspond to cell viability values upon idelalisib exposure with no siRNA infection. Data derived from three independent experiments, error bars represent standard deviation of the mean. Statistically significant differences when compared to parental or resistant are highlighted in yellow (Z-test P<0.05).

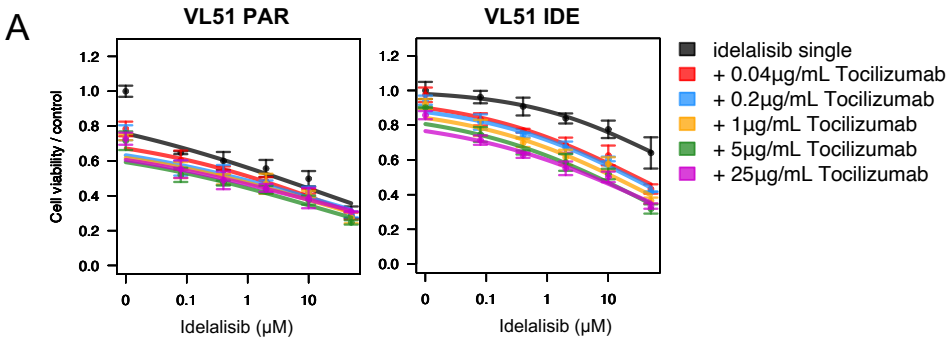

p-value from a Z-test comparing each combination to idelalisib single		
combination	Parental	Resistant
0.04μg/mL tocilizumab	0.369	0.033
0.2μg/mL tocilizumab	0.282	0.015
1μg/mL tocilizumab	0.208	0.006
5μg/mL tocilizumab	0.129	0.003
25μg/mL tocilizumab	0.207	0.001

Statistically significant differences highlighted in yellow

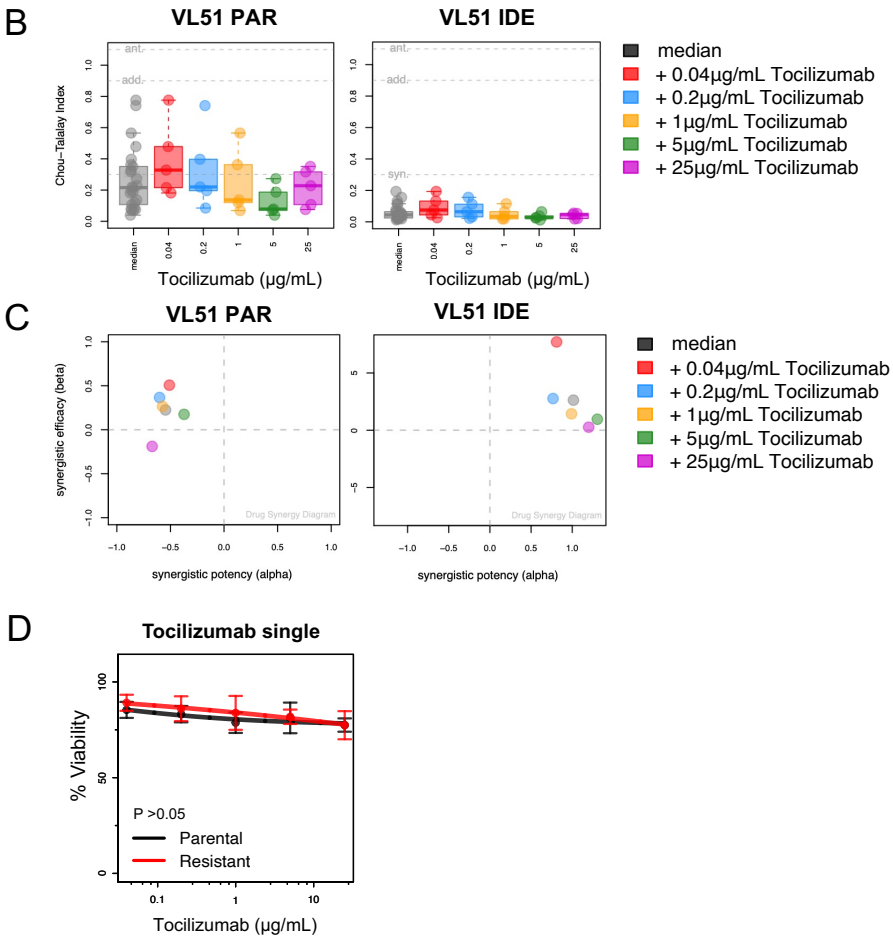

Figure S9. (A) Cell viability for the combination of idelalisib and the IL6 blocking antibody tocilizumab in parental and resistant by MTT assay (72h). Bars correspond to the mean of two independent experiments. Error bars represent standard deviation of the mean. Table contains p-values from a Z-test comparing each combination to idelalisib as single agent. Statistically significant values highlighted in yellow. The benefit of the combination was assessed both as synergism according to the Chou-Talalay combination index (B) (23) and as potency (x-axis) and efficacy (y-axis) according to the MuSyC algorithm (C) (3). VL51 PAR: parental, VL51 IDE: resistant. (D) Sensitivity to tocilizumab as a single agent in parental (black) and resistant (red). P for p-value from a Z-test comparing parental to resistant.

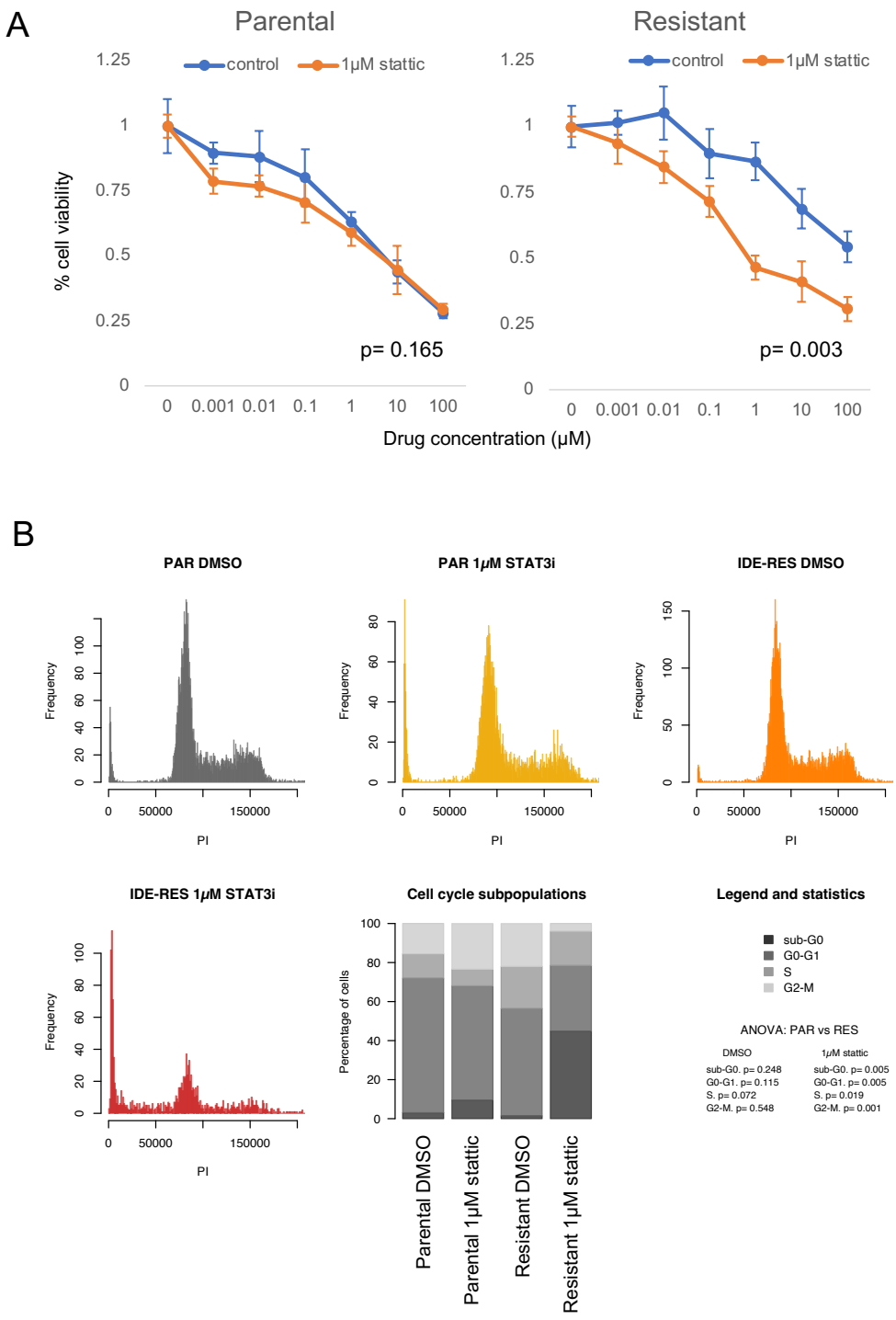

Figure S10. Cell viability (A, MTT assay) and cell cycle phases (B) for the combination of idelalisib with DMSO or with 1μM of the STAT3 inhibitor stattic in parental and resistant. Data derived from the mean of two independent experiments. Error bars represent standard deviation of the mean. P values from Z-test (drug-response curves), or from ANOVA (cell cycle) for statistically significant differences comparing parental to resistant (P <0.05).

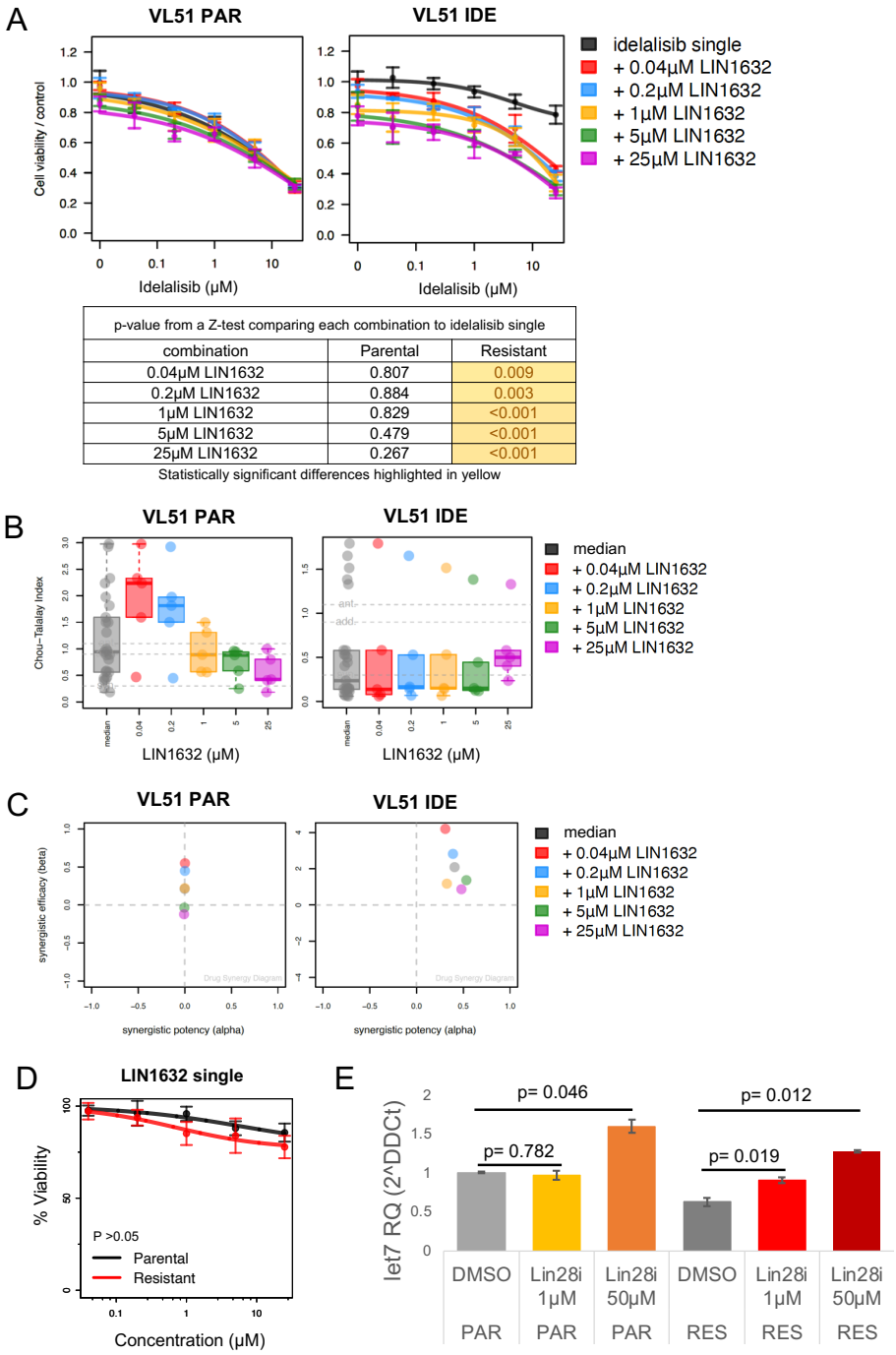

p-value from a Z-test comparing each combination to idelalisib single

combination	Parental	Resistant
0.04μM LIN1632	0.807	0.009
0.2μM LIN1632	0.884	0.003
1μM LIN1632	0.829	<0.001
5μM LIN1632	0.479	<0.001
25μM LIN1632	0.267	<0.001

Statistically significant differences highlighted in yellow

Figure S11. (A) Cell viability for the combination of idelalisib and the LIN28 inhibitor LIN1632 in parental and resistant by MTT assay (72h). Bars correspond to the mean of two independent experiments. Error bars represent standard deviation of the mean. Table contains p-values from a Z-test comparing each combination to idelalisib as single agent. Statistically significant values highlighted in yellow. The benefit of the combination was assessed both as synergism according to the Chou-Talalay combination index (B) (23) and as potency (x-axis) and efficacy (y-axis) according to the MuSyC algorithm (C) (3). VL51 PAR: parental, VL51 IDE: resistant. (D) Sensitivity to LIN1632 as a single agent in parental (black) and resistant (red). P for p-value from a Z-test comparing parental to resistant. (E) Expression levels of let-7g microRNA was evaluated by real-time PCR (delta-delta Ct method, TaqMan probe) in VL51 parental (three bars on the left, PAR) and resistant (three bars on the right, RES) cells upon 1μM or 50μM of LIN1632. Bars correspond to the mean of two independent experiments. Error bars represent standard deviation of the mean. P for p-value from a t-test comparing LIN1632 treatments to DMSO.

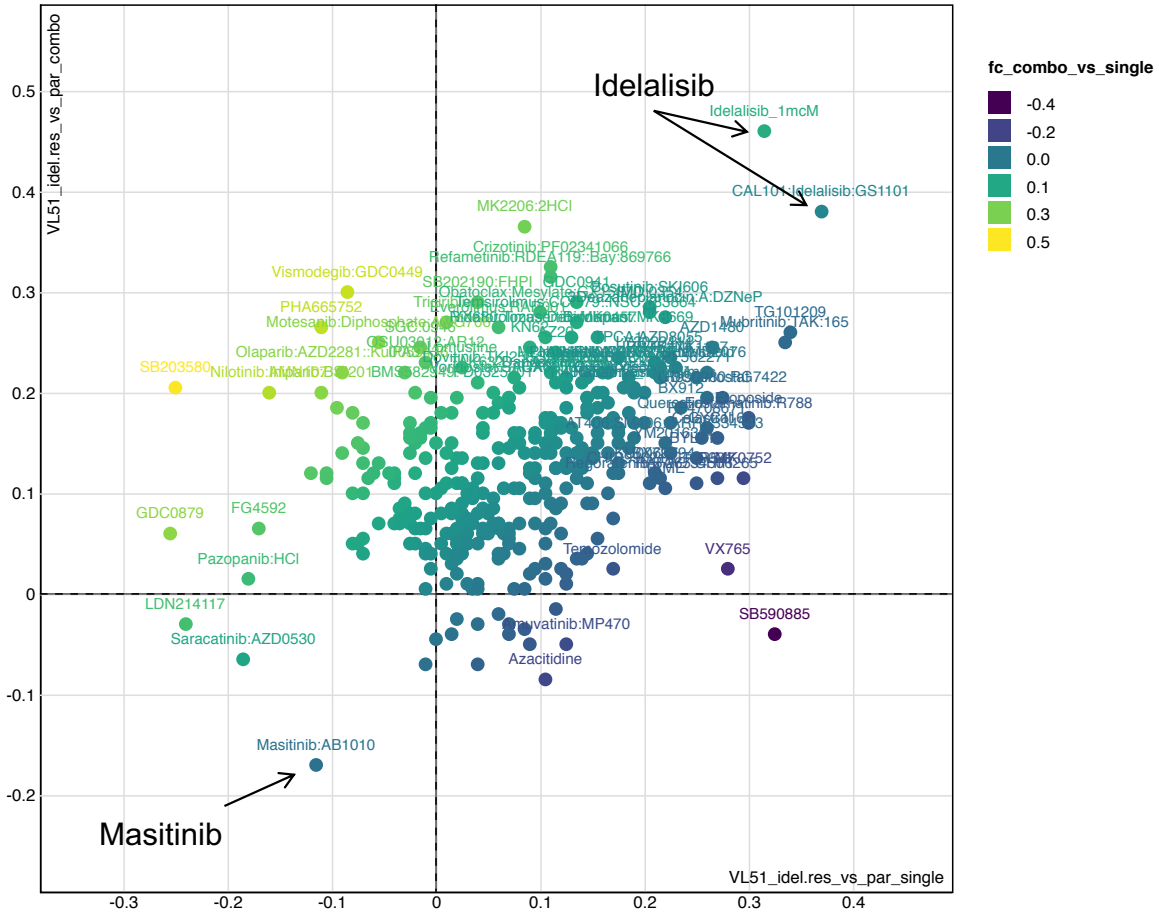

Figure S12. Resistant in parallel with parental clones of VL51 cell line were exposed to a library of 348 compounds alone (single, 1µM) or in combination with 1µM idelalisib (combo) for 72h. Cell viability was measured by MTT assay (72h). Yellow for benefit in combo, purple benefit in single treatment.

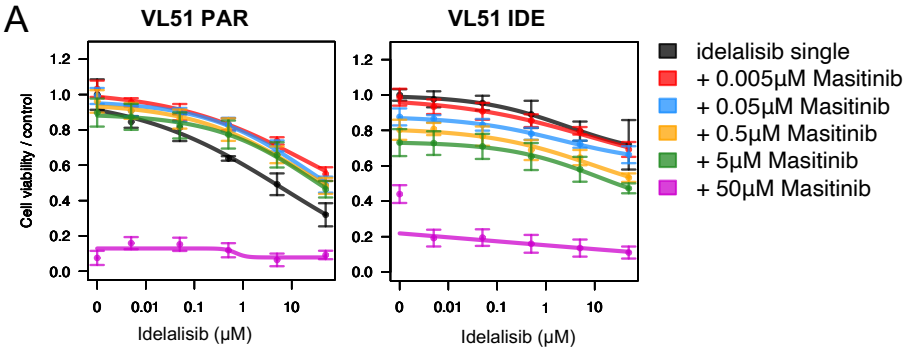

p-value from a Z-test comparing each combination to idelalisib single		
combination	Parental	Resistant
0.04μM masitinib	0.096	0.498
0.2μM masitinib	0.166	0.024
1μM masitinib	0.272	0.001
5μM masitinib	0.429	<0.001
25μM masitinib	<0.001	<0.001

Statistically significant differences highlighted in yellow

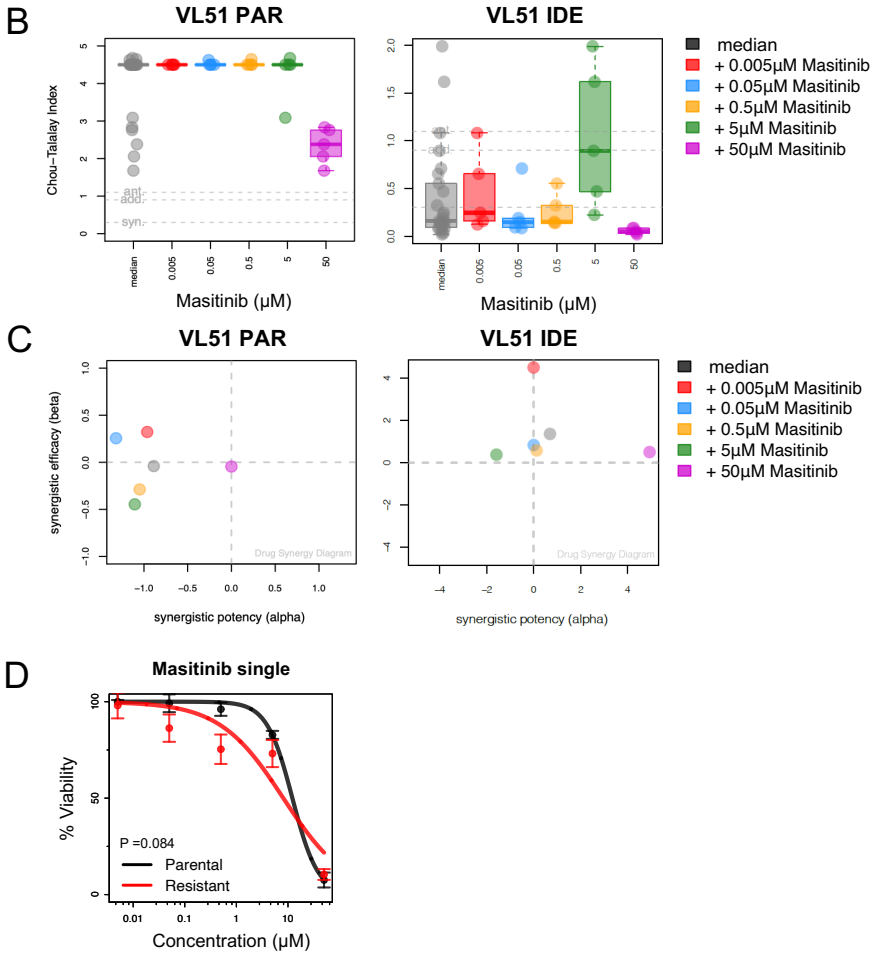

Figure S13. (A) Cell viability for the combination of idelalisib and the PDGFR inhibitor masitinib in parental and resistant by MTT assay (72h). Bars correspond to the mean of two independent experiments. Error bars represent standard deviation of the mean. Table contains p-values from a Z-test comparing each combination to idelalisib as single agent. Statistically significant values highlighted in yellow. The benefit of the combination was assessed both as synergism according to the Chou-Talalay combination index (B) (23) and as potency (x-axis) and efficacy (y-axis) according to the MuSyC algorithm (C) (3). VL51 PAR: parental, VL51 IDE: resistant. (D) Sensitivity to masitinib as a single agent in parental (black) and resistant (red). P for p-value from a Z-test comparing parental to resistant.

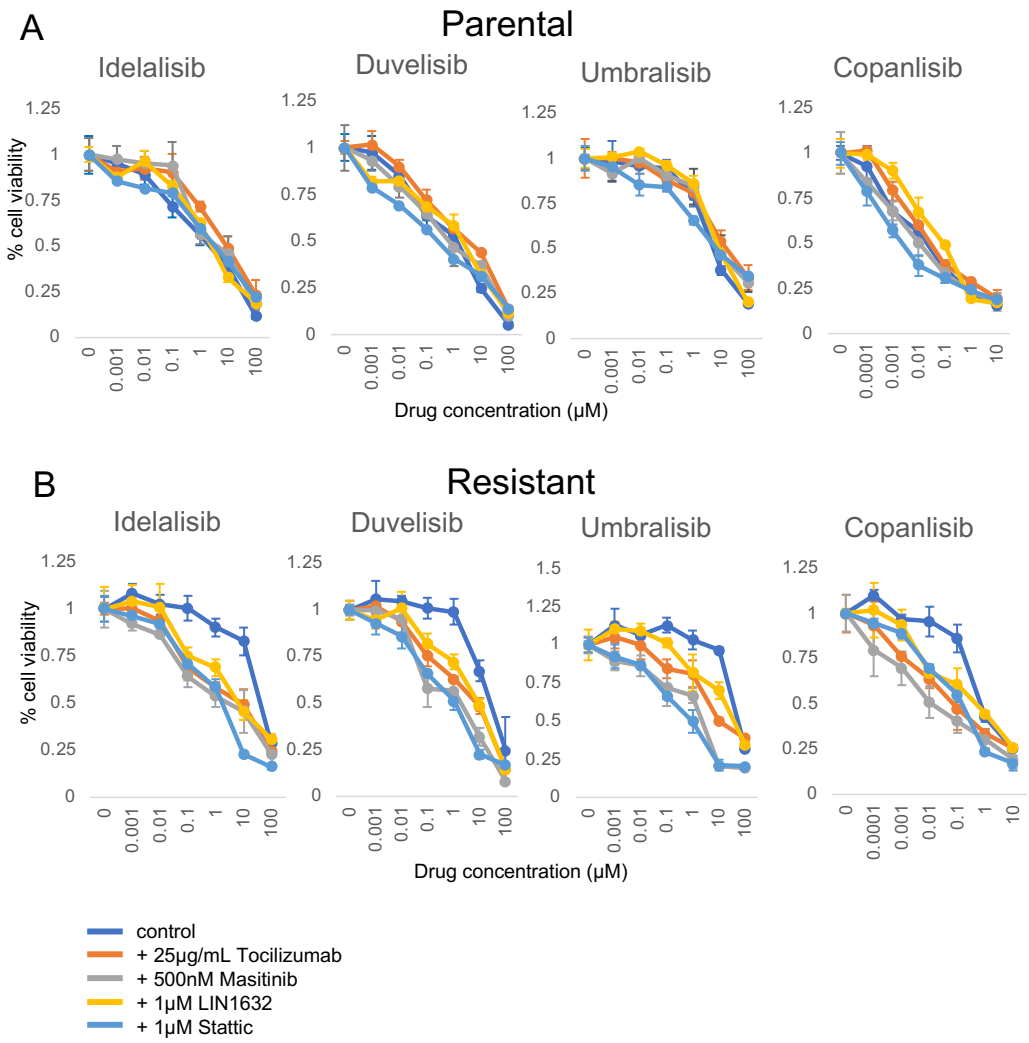

p-values from Z-test testing change in sensitivity to PI3K inhibitors upon each treatment compared to control (DMSO)					
Clone	Treatment	Idelalisib	Duvelisib	Umbralisib	Copanlisib
Parental	Tocilizumab	0.3062	0.3426	0.2173	0.0709
Parental	Masitinib	0.4136	0.4796	0.4985	0.3680
Parental	LIN1632	0.5000	0.4921	0.4670	0.4006
Parental	Stattic	0.4963	0.3594	0.4476	0.3164
Resistant	Tocilizumab	0.0238	0.0258	0.0431	0.0341
Resistant	Masitinib	0.0108	0.0144	0.0122	0.0299
Resistant	LIN1632	0.0259	0.0021	0.0538	0.0662
Resistant	Stattic	0.0104	0.0051	0.0067	0.0030

Statistically significant differences highlighted in yellow

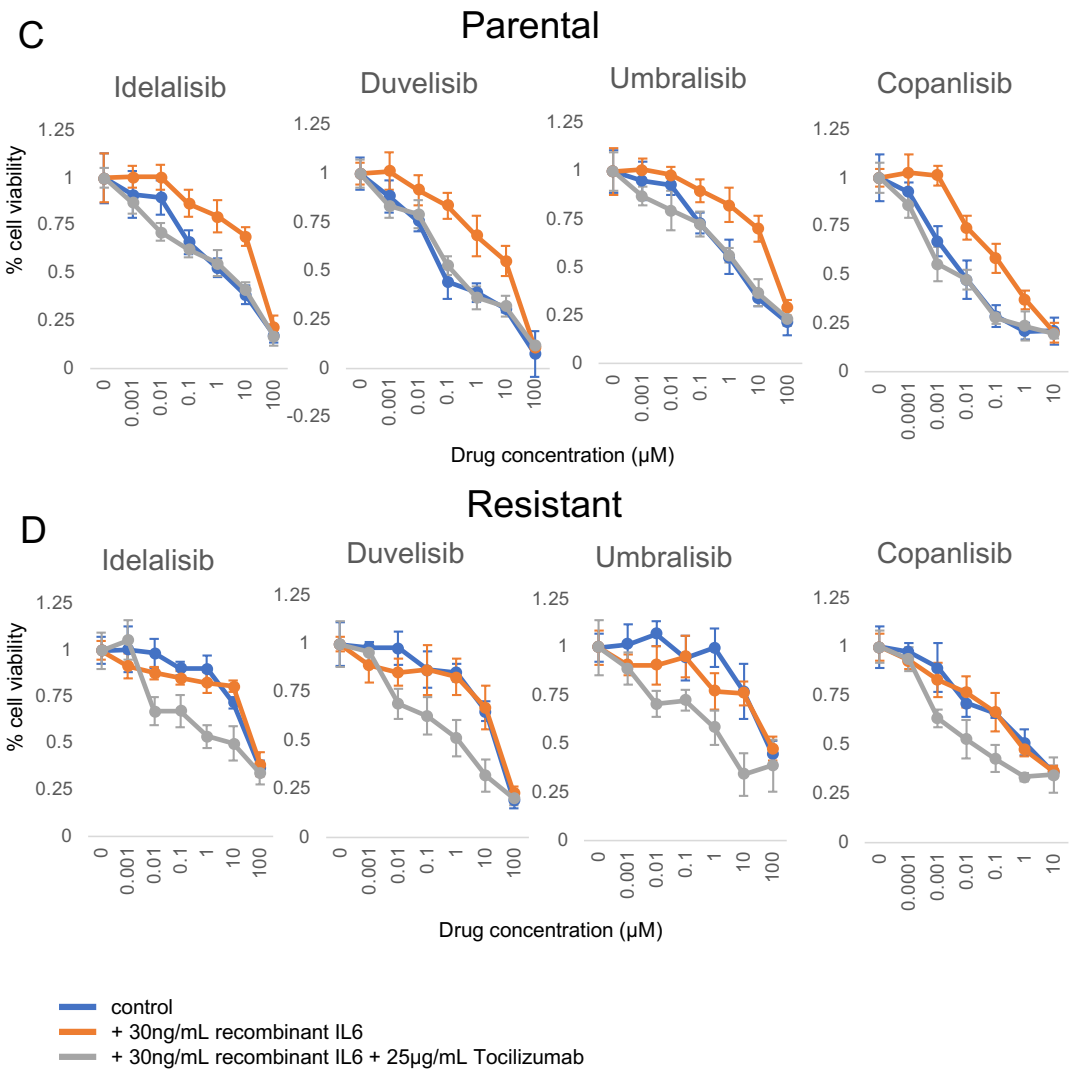

p-values from Z-test testing change in sensitivity to PI3K inhibitors upon each treatment compared to control (DMSO)					
Clone	Treatment	Idelalisib	Duvelisib	Umbralisib	Copanlisib
Parental	IL6 stimulation	0.0108	0.0105	0.0257	0.0170
Parental	IL6 + tocilizumab	0.3118	0.4659	0.3512	0.2233
Resistant	IL6 stimulation	0.2968	0.2809	0.1246	0.5078
Resistant	IL6 + tocilizumab	0.0391	0.0242	0.0086	0.0146

Statistically significant differences highlighted in yellow

Figure S14. Cell viability was evaluated by MTT assay (72h)**.** VL51 parental (A) and resistant (B) cells upon idelalisib, copanlisib, duvelisib and umbralisib, alone (cnt, dark blue), or in combination with tocilizumab (anti-IL-6R blocking antibody 25μg/mL, orange), masitinib (PDGFR inhibitor, 500 nM, grey), LIN1632 (LIN28 inhibitor, 1μM, yellow), or stattic (STAT3 inhibitor, 1μM, light blue). VL51 parental (C) and resistant (D) cells upon idelalisib, copanlisib, duvelisib and umbralisib, alone (cnt, blue), or upon stimulation with recombinant IL-6 (30ng/mL), or IL-6 stimulation in presence of tocilizumab (25μg/mL, grey). Error bars correspond to standard deviation of the mean. Data derived from two independent experiments. Statistically significant differences were evaluated by Z-test comparing each treatment to control (DMSO). Values on tables correspond to p-values from the Z-test, $p<0.05$ was considered significant (highlighted in yellow).

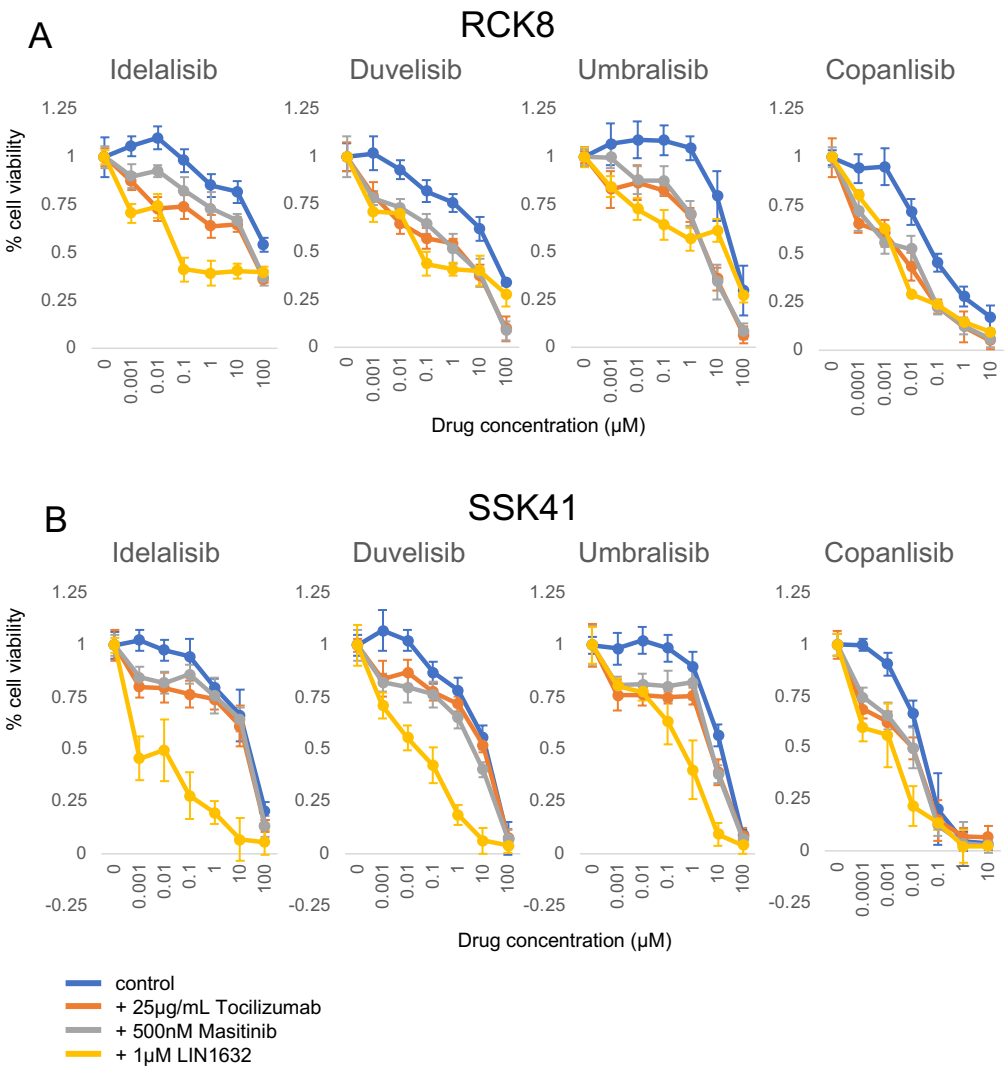

p-values from Z-test testing change in sensitivity to PI3K inhibitors upon each treatment compared to control (DMSO)					
Clone	Treatment	Idelalisib	Duvelisib	Umbralisib	Copanlisib
RCK8	Tocilizumab	0.0137	0.0117	0.0077	0.0204
RCK8	Masitinib	0.0428	0.0308	0.0054	0.0163
RCK8	LIN1632	0.0012	0.0273	0.0100	0.0149
SSK41	Tocilizumab	0.0453	0.0771	0.0120	0.0283
SSK41	Masitinib	0.0568	0.0326	0.0315	0.0317
SSK41	LIN1632	0.0022	0.0081	0.0086	0.0119

Statistically significant differences highlighted in yellow

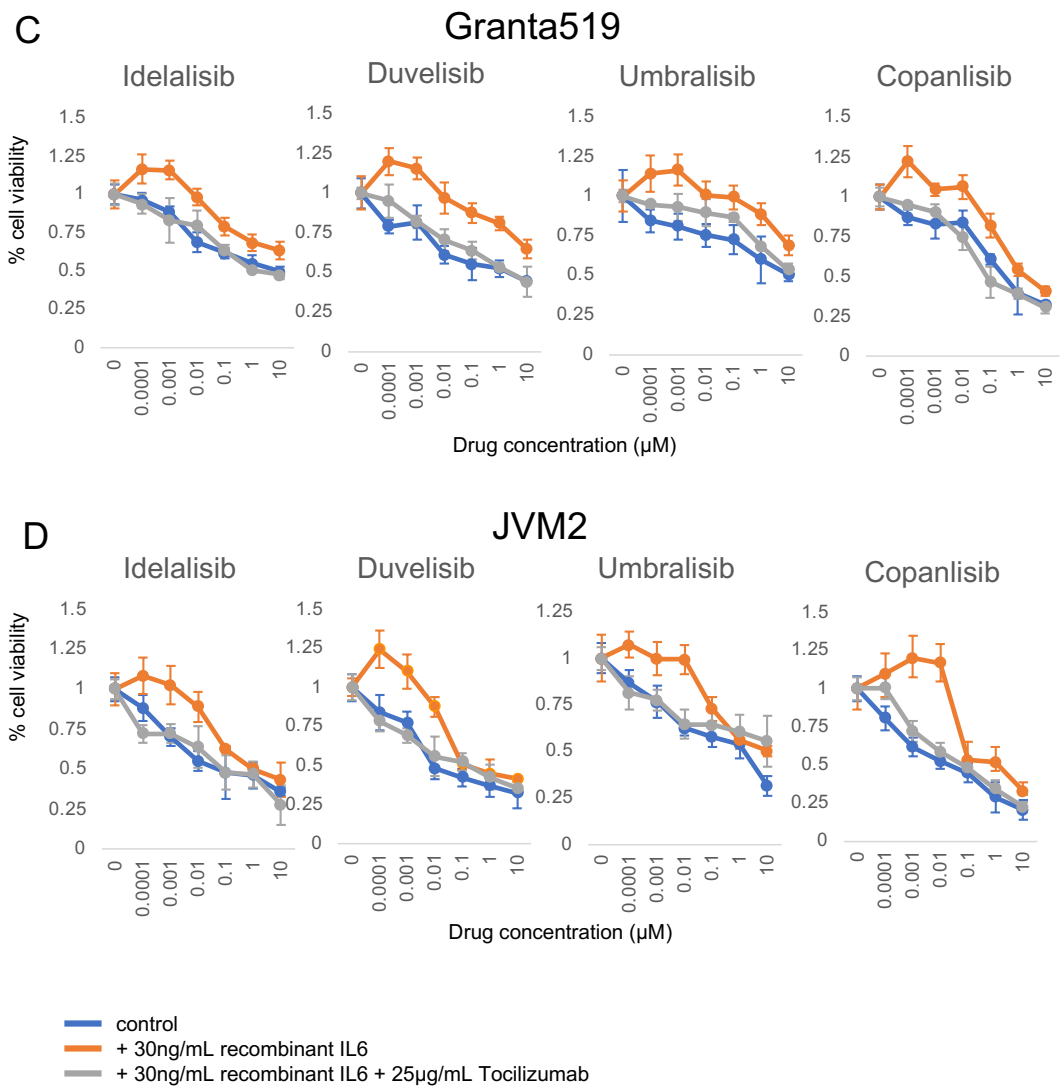

p-values from Z-test testing change in sensitivity to PI3K inhibitors upon each treatment compared to control (DMSO)					
Clone	Treatment	Idelalisib	Duvelisib	Umbralisib	Copanlisib
Granta519	IL6 stimulation	0.0355	0.0050	0.0014	0.0467
Granta519	IL6 + tocilizumab	0.8985	0.5680	0.2624	0.6505
JVM2	IL6 stimulation	0.0280	0.0349	0.0250	0.0197
JVM2	IL6 + tocilizumab	0.5952	0.5152	0.2124	0.6040

Statistically significant differences highlighted in yellow

Figure S15. Cell viability was evaluated by MTT assay (72h)**.** Primary resistant RCK8 (A) and SSK41 (B) lines upon idelalisib, copanlisib, duvelisib and umbralisib, alone (cnt, blue), or in combination with tocilizumab (anti-IL-6R blocking antibody 25μg/mL, orange), masitinib (PDGFR inhibitor, 500 nM, grey), or LIN1632 (LIN28 inhibitor, 1μM, yellow). Primary sensitive Granta519 (C) and JVM2 (D) lines upon idelalisib, copanlisib, duvelisib and umbralisib, alone (cnt, blue), or upon stimulation with recombinant IL-6 (30ng/mL), or IL-6 stimulation in presence of tocilizumab (25μg/mL, grey). Error bars correspond to standard deviation of the mean. Data derived from two independent experiments. Statistically significant differences were evaluated by Z-test comparing each treatment to control (DMSO). Values on tables correspond to p-values from the Z-test, $p<0.05$ was considered significant (highlighted in yellow).

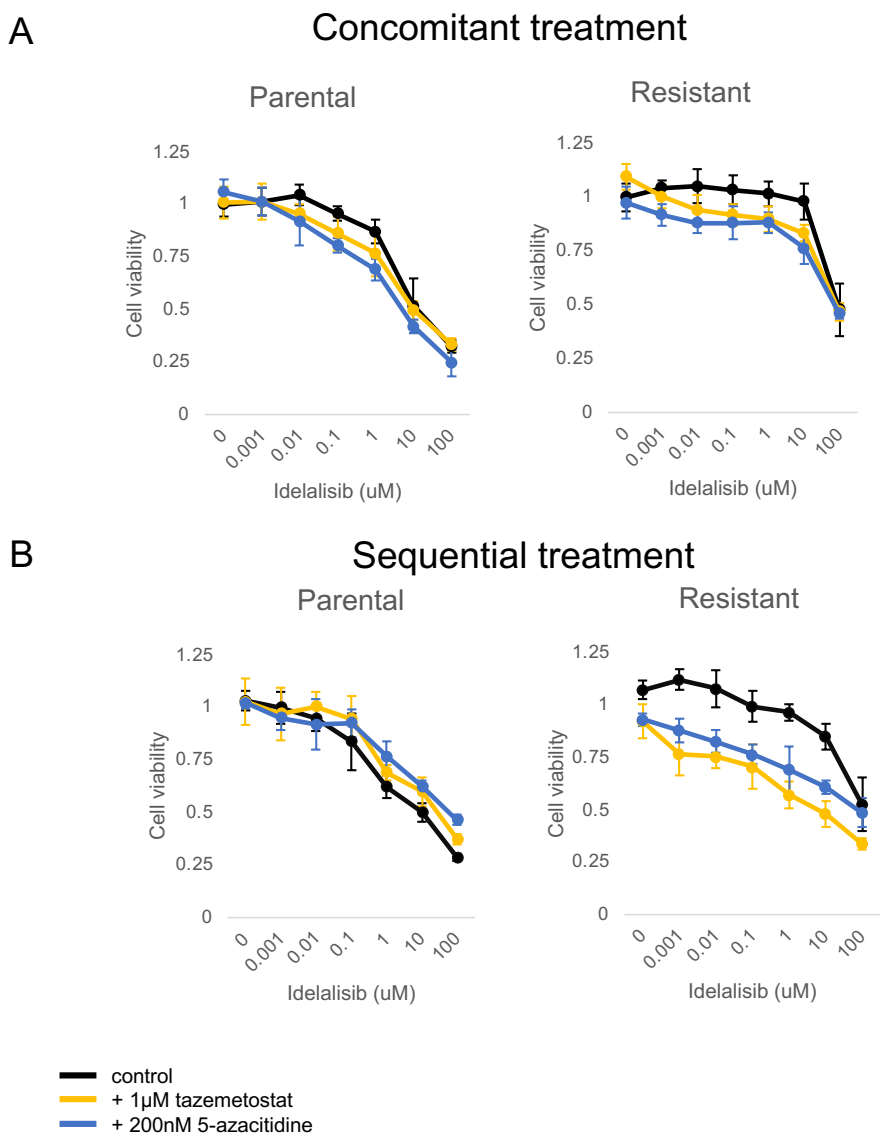

p-values from Z-test testing change in sensitivity to PI3K inhibitors upon each treatment compared to control (DMSO)			
Clone	Treatment	1μM tazemetostat	200nM 5-Azacitidine
Parental	concomitant	0.4246	0.2230
Parental	sequential	0.1607	0.1150
Resistant	concomitant	0.0927	0.0571
Resistant	sequential	0.0017	0.0068

Statistically significant differences highlighted in yellow

Figure S16. Cell viability was evaluated by MTT assay (72h). VL51 parental (left) or resistant (right) were exposed to DMSO (0.01%, cnt, black), 5-azacitidine (200nM, blue) or tazemetostat (1μM, yellow), given concomitantly (A) or five days before idelalisib (B). Error bars correspond to standard deviation of the mean. Data derived from two independent experiments. Statistically significant differences were evaluated by Z-test comparing each treatment to control (DMSO). Values on tables correspond to p-values from the Z-test, $p<0.05$ was considered significant (highlighted in yellow).

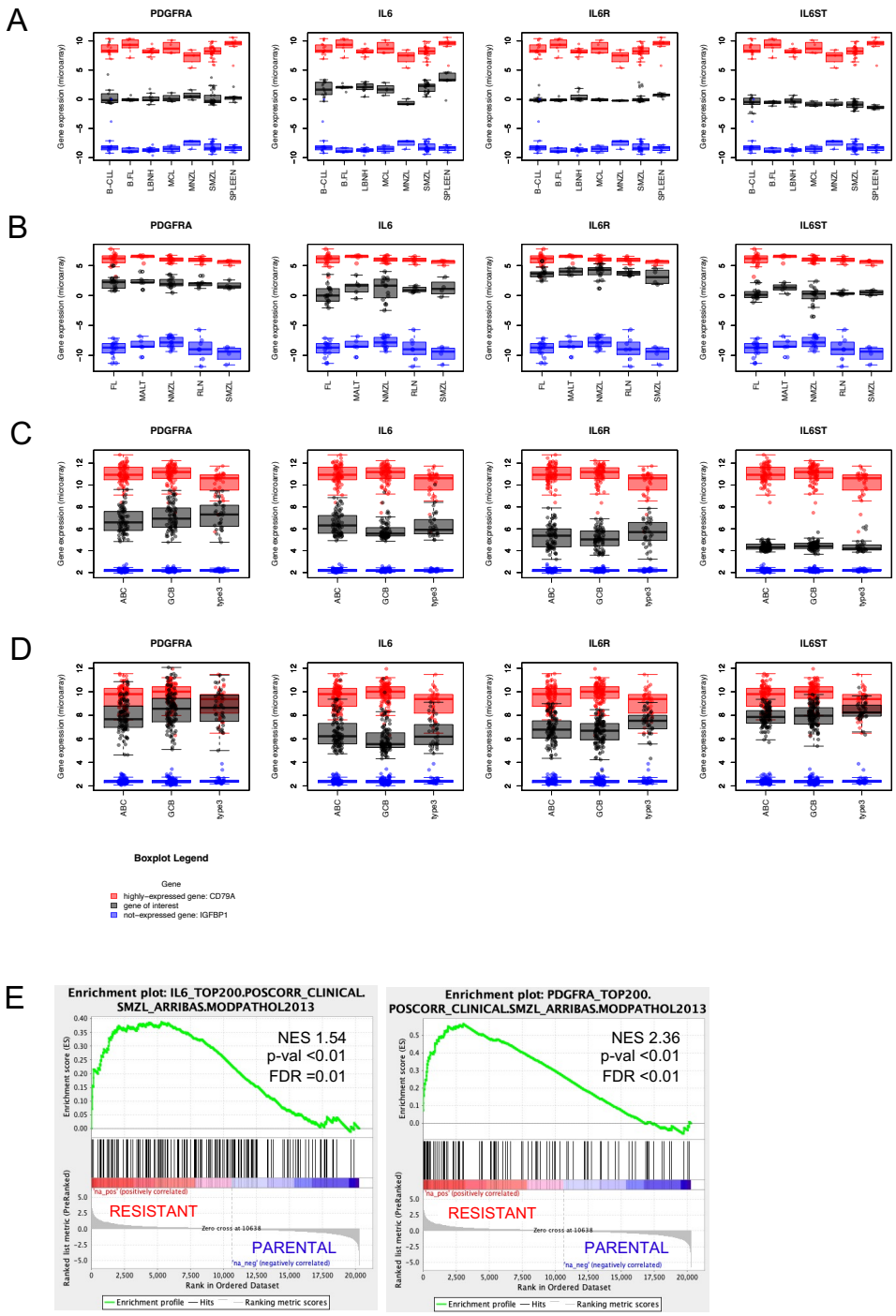

Figure S17. Factors associated with resistance to idelalisib in cell lines are expressed in clinical specimens. Expression levels of genes related to idelalisib resistance were studied across different subtypes of B cell lymphoma: (A) n=80 (24); (B) n=48 (25). B-CLL: chronic lymphocytic leukemia, B.FL: follicular lymphoma, LBNH: non-specified non-Hodgkin B cell lymphoma, MALT: MZL of the mucosa associated tissue, MCL: Mantle cell lymphoma, NMZL: nodal marginal zone lymphoma, SMZL: splenic marginal zone lymphoma. Expression levels of genes related to idelalisib resistance were studied across the subtypes of diffuse large B cell lymphoma (DLBCL, two series: (C) n=181 and (D) n=223 from GSE10846 (26). ABC: activated B cell like DLBCL, GCB: germinal center B cell like DLBCL, type3: type3 DLBCL. Red for highly expressed gene in B cells (CD79A), blue for not expressed gene in B cells (IGFBP1), black for the gene of interest. (E) Gene set enrichment analyses comparing resistant versus parental for the top-200 genes positively correlated genes with *IL6* and *PDGFRA* in SMZL clinical specimens. NES: normalized enrichment score, p-val: nominal p-value, FDR: false discovery rate.

References

1. Smirnov P, Safikhani Z, El-Hachem N, et al. PharmacoGx: an R package for analysis of large pharmacogenomic datasets. Bioinformatics. 2016;32(8):1244-6.

2. Spriano F, Chung EYL, Gaudio E, et al. The ETS Inhibitors YK-4-279 and TK-216 Are Novel Antilymphoma Agents. Clin Cancer Res. 2019;25(16):5167-5176.

3. Meyer CT, Wooten DJ, Paudel BB, et al. Quantifying Drug Combination Synergy along Potency and Efficacy Axes. Cell Syst. 2019;8(2):97-108 e16.

4. Hicks SW, Tarantelli C, Wilhem A, et al. The novel CD19-targeting antibody-drug conjugate huB4-DGN462 shows improved anti-tumor activity compared to SAR3419 in CD19-positive lymphoma and leukemia models. Haematologica. 2019;104(8):1633-1639.

5. Tissino E, Benedetti D, Herman SEM, et al. Functional and clinical relevance of VLA-4 (CD49d/CD29) in ibrutinib-treated chronic lymphocytic leukemia. The Journal of experimental medicine. 2018;215(2):681-697.

6. Hahne F, LeMeur N, Brinkman RR, et al. flowCore: a Bioconductor package for high throughput flow cytometry. BMC Bioinformatics. 2009;10:106.

7. Cascione L, Rinaldi A, Bruscaggin A, et al. Novel insights into the genetics and epigenetics of MALT lymphoma unveiled by next generation sequencing analyses. Haematologica. 2019;104(12):e558-e561.

8. Moran S, Arribas C, Esteller M. Validation of a DNA methylation microarray for 850,000 CpG sites of the human genome enriched in enhancer sequences. Epigenomics. 2016;8(3):389-99.

9. Andrews S. FastQC A Quality Control tool for High Throughput Sequence Data. 2014.

10. Li H, Durbin R. Fast and accurate long-read alignment with Burrows-Wheeler transform. Bioinformatics. 2010;26(5):589-95.

11. Li H, Handsaker B, Wysoker A, et al. The Sequence Alignment/Map format and SAMtools. Bioinformatics. 2009;25(16):2078-9.

12. Van der Auwera GA, O'Connor BD. Genomics in the Cloud. O'Reilly Media, Inc.; 2020. ISBN: 9781491975190.

13. DePristo MA, Banks E, Poplin R, et al. A framework for variation discovery and genotyping using next-generation DNA sequencing data. Nature genetics. 2011;43(5):491-8.

14. Wang K, Li M, Hakonarson H. ANNOVAR: functional annotation of genetic variants from high-throughput sequencing data. Nucleic Acids Res. 2010;38(16):e164.

15. Robinson JT, Thorvaldsdóttir H, Winckler W, et al. Integrative genomics viewer. Nat Biotechnol. 2011;29(1):24-6.

16. Auton A, Brooks LD, Durbin RM, et al. A global reference for human genetic variation. Nature. 2015;526(7571):68-74.

17. Tate JG, Bamford S, Jubb HC, et al. COSMIC: the Catalogue Of Somatic Mutations In Cancer. Nucleic Acids Res. 2019;47(D1):D941-d947.

18. Liberzon A, Subramanian A, Pinchback R, et al. Molecular signatures database (MSigDB) 3.0. Bioinformatics. 2011;27(12):1739-40.

19. Subramanian A, Tamayo P, Mootha VK, et al. Gene set enrichment analysis: a knowledge-based approach for interpreting genome-wide expression profiles. Proc Natl Acad Sci U S A. 2005;102(43):15545-50.

20. Martin M. Cutadapt removes adapter sequences from high-throughput sequencing reads [next generation sequencing; small RNA; microRNA; adapter removal]. EMBnetjournal. 2011 2011;17(1):10-12.

21. Kozomara A, Birgaoanu M, Griffiths-Jones S. miRBase: from microRNA sequences to function. Nucleic Acids Res. 2019;47(D1):D155-d162.

22. Liao Y, Smyth GK, Shi W. featureCounts: an efficient general purpose program for assigning sequence reads to genomic features. Bioinformatics. 2014;30(7):923-30.

23. Chou TC. Drug combination studies and their synergy quantification using the Chou-Talalay method. Cancer research. 2010;70(2):440-6.

24. Arribas AJ, Gomez-Abad C, Sanchez-Beato M, et al. Splenic marginal zone lymphoma: comprehensive analysis of gene expression and miRNA profiling. Modern pathology : an official journal of the United States and Canadian Academy of Pathology, Inc. 2013;26(7):889-901.

25. Arribas AJ, Campos-Martín Y, Gómez-Abad C, et al. Nodal marginal zone lymphoma: gene expression and miRNA profiling identify diagnostic markers and potential therapeutic targets. Blood. 2012;119(3):e9-e21.

26. Lenz G, Wright G, Dave SS, et al. Stromal gene signatures in large-B-cell lymphomas. N Engl J Med. 2008;359(22):2313-23.